

Article

Comparison of Mechanical and Low-Frequency Dielectric Properties of Thermally and Thermo-Mechanically Aged Low Voltage CSPE/XLPE Nuclear Power Plant Cables

Ramy S. A. Afia ^{1,2} , Ehtasham Mustafa ^{2,3}  and Zoltán Ádám Tamus ^{2,*} 

¹ Department of Electrical Power and Machines Engineering, Helwan University, Helwan 11792, Egypt; ramysaad@h-eng.helwan.edu.eg

² Department of Electric Power Engineering, Faculty of Electrical Engineering and Informatics, Budapest University of Technology and Economics, H-1111 Budapest, Hungary; mustafa.ehtasham@vet.bme.hu

³ Department of Electrical Engineering, Faculty of Engineering and Technology, Gomal University, Dera Ismail Khan 29050, Pakistan

* Correspondence: tamus.adam@vik.bme.hu; Tel.: +36-1-463-2780

Abstract: During the service period of low-voltage nuclear cables, multiple stresses influence the aging of polymeric materials of cables. Thermal and radiation stresses are considered service aging factors in qualification tests, while the standards usually do not prescribe mechanical stress. CSPE/XLPE insulated nuclear cable samples were exposed to thermal and combined thermo-mechanical aging for more than 1200 h at 120 °C. The real and imaginary parts of permittivity were measured in the 200 μHz to 50 mHz range as dielectric properties. The Shore D hardness of the samples was measured to analyze the mechanical characteristics of the cable. To characterize the dielectric spectrum, derived quantities, namely central real and imaginary permittivities and real and imaginary permittivities' central frequencies were calculated. The change of dielectric spectra did not show a clear trend with aging, but the imaginary permittivity's central frequency was higher by 0.5 mHz in the case of thermo-mechanically aged samples. The Shore D hardness was also higher on the thermo-mechanically aged samples. These findings show the combined aging has a higher impact on the insulation properties. Hence, involving the mechanical stress in the aging procedure of cable qualification enables the design of more robust cables in a harsh environment.

Keywords: nuclear power plant; thermal degradation; thermal-mechanical aging; low-voltage cables; polymer degradation; dielectric spectroscopy; hardness



Citation: Afia, R.S.A.; Mustafa, E.; Tamus, Z.Á. Comparison of Mechanical and Low-Frequency Dielectric Properties of Thermally and Thermo-Mechanically Aged Low Voltage CSPE/XLPE Nuclear Power Plant Cables. *Electronics* **2021**, *10*, 2728. <https://doi.org/10.3390/electronics10222728>

Academic Editor: Davide Astolfi

Received: 12 October 2021

Accepted: 4 November 2021

Published: 9 November 2021

Publisher's Note: MDPI stays neutral with regard to jurisdictional claims in published maps and institutional affiliations.



Copyright: © 2021 by the authors. Licensee MDPI, Basel, Switzerland. This article is an open access article distributed under the terms and conditions of the Creative Commons Attribution (CC BY) license (<https://creativecommons.org/licenses/by/4.0/>).

1. Introduction

In 2020, the built-in nuclear-generating capacity was 393 GW (electrical), and its contribution to electricity generation is expected to increase. In the highest case predictions, the world's nuclear capacity will be doubled to 792 GW by 2050, keeping its almost 5% ratio [1]. Hence, nuclear power will keep its important role in power generation for decades, and the current nuclear power plants' (NPPs') designed lifetime is potentially extended to 80 years [2]. During this long period, the safe and reliable operation of NPPs in normal service and design basis events (DBEs) require safety-related equipment performance to meet their designed requirements. The equipment qualification is the procedure when safety-related equipment performance is tested in all operational states and accident conditions [3]. Since the cabling condition plays a key role in the reliable operation of safety systems, the safety-related cables as system components are also subject to the qualification which the test procedure is described by standards [4]. More the 1000 miles of cable installed typically in a pressurized water reactor (PWR), low-voltage (LV) power cables account for only 15% of the total LV cables deployed in the NPPs [5]. Still, they are highly important as they supply motors and pumps related to nuclear safety. The structure of these

cables varies with the application. These power cables are multi- or single conductors with or without shielding and have different polymeric components for core insulation, jacket, and filling material [6–9]. During operation in the NPP environment, these LV cables are exposed to numerous stresses, thermal, radiation, electrical, and mechanical, which cause degradation in these polymeric materials [10]. The electrical and thermal stresses are the prominent aging factors for the high-voltage (HV) and medium-voltage (MV) cables [11]. For the LV cables, elevated temperature and radiation could be the major factors, along with the chemical contamination and mechanical stresses in some cases [10,12].

Considering that the operational stresses affect the cables' functionality, the qualification procedure includes the simulation of aging in normal service conditions before DBE and post-DBE functionality tests. Although mechanical stress as pressing with a cable cleat, and low bending radius, can appear in operation, the standards do not prescribe any mechanical stress during the accelerated aging that simulates operation conditions [13]. Nevertheless, the bending with a low radius is used to demonstrate a lack of embrittlement and adequate flexibility after aging [4]. The impact of mechanical stress on the degradation of the polymers is well known, and numerous studies have investigated the effects of mechanical stress on the functionality of the polymer insulating materials [14]. However, as the degradation or aging of the polymeric material is a multi-factor phenomenon, thermal stress has more importance than other stresses. However, the effect of the simultaneous presence of mechanical stress and thermal stress on high-voltage cables has been investigated since the 1980s [15], the topic still has to be explored in the case of the NPPs environment.

According to the robust design principle, the product performance can be improved by minimizing performance variations caused by uncontrollable parameters (noise factors) or design variables (control factors) [16]. The robust approach is widely used in the design of NPP control systems, electrical equipment, and machines [17–23]. Hence, considering NPP cable as a product, if the mechanical stress is not prescribed as an aging parameter in qualification, this can be regarded as a noise factor and can cause uncertainty in the cable performance. If the mechanical stress is involved in the aging procedure, the performance uncertainty caused by this factor can be minimized. Therefore, the purpose of this study is to compare the mechanical and dielectric properties of cable samples subjected to thermal only and combined thermal and mechanical aging.

The subject of the investigation is a single-core cross-linked polyethylene (XLPE) insulated and chlorosulphonated polyethylene (CSPE) jacketed NPP power cable. One group of cables was only thermally and the other thermo-mechanically aged. The change of dielectric properties was measured by low-frequency dielectric spectroscopy. The reason for the application of this technique in this study is that dielectric spectroscopy as condition monitoring for NPP cables has recently become a focus of interest because of its non-destructivity. Several studies show promising results, and their future expansion is likely [11,12,24–31]. From the results of dielectric spectroscopy measurement, deduced quantities were introduced because assigning one measure to the whole low-frequency spectrum makes it easier to analyze the changing of the dielectric spectrum with aging. The mechanical properties were measured using Shore D hardness, which is a simplified indenter measurement. The indenter type measurements are widely and effectively used for the aging monitoring of NPP cables [32–34]. The results of the thermally and thermo-mechanically aged groups were compared to determine the degradation caused by combined stress over the simple thermal aging.

This paper has been organized, as Section 2 elaborates the cable sample, aging stresses, the electrical and mechanical measurement. The results of the measurement are given in Section 3. Section 4 explains the measurement results, and the concluding remarks are provided in Section 5.

2. Materials and Methods

2.1. Specimens

A Firewall III radiation-resistant Class 1E low-voltage (600 V) NPP unshielded power cable (RSCC Wire and Cable, East Granby, CT, USA) under investigation is shown in Figure 1. The cable consisted of three parts: annealed, tin-coated copper conductor with a cross-sectional area of 6 AWG (13.3 mm²), cross-linked polyethylene (XLPE) core insulation having a thickness of 45 mils (1.143 mm), and chlorosulphonated polyethylene (CSPE) jacket with 30 mils (0.762 mm) thickness. The overall diameter of the cable was 0.34 inches (8.636 mm). Under the International Atomic Energy Agency's (IAEA's) guidelines [35] and as expressed in Figure 1, 1 cm and 3 cm of the insulation and jacket were removed from both sides of the cable sample, respectively. The cable sample was 0.5 m in length for the experiments.



Figure 1. The LV unshielded NPP cable under consideration. A—Tin-coated copper, B—XLPE insulation, C—CSPE jacket.

2.2. Accelerated Aging

2.2.1. Thermal Aging

The cable samples were exposed to 120 °C accelerated thermal agings in an air-circulating oven for seven different periods: 176, 338, 512, 784, 912, 1056, and 1248 h. Applying these aging parameters is because the 120 °C aging temperature was also used for benchmark analysis of this cable type in the IAEA Coordinated Research Project [35]. Moreover, elongation at break data for the CSPE jacket are also available for these aging times in [35]. The cable samples in the oven are shown in Figure 2a.



(a)



(b)

Figure 2. Cable samples in the oven for (a) thermal aging; (b) thermo-mechanical aging.

2.2.2. Thermo-Mechanical Aging

According to the IEEE standard, the cable samples were bent on a mandrel with an outer diameter of 15 cm for the thermo-mechanical (T-M) simultaneous aging [4].

Then the cable samples were placed in the air circulated oven at a temperature of 120 °C. The cables were exposed to simultaneous aging for 176, 338, 507, 779, 907, 1051, and 1243 h (Figure 2b). After each aging period, the samples were removed from the cylinder and straightened for measurements. After the measurements, the samples were bent on the cylinder again. Then, they inserted back to the aging chamber for the next round.

2.3. Dielectric Spectroscopy Measurement

Since the subject of the investigation is a single core unshielded power cable having a jacket and core insulation also, this cable structure can be considered a layered insulation arrangement. The most dominant polarization process in layered insulations is interfacial polarization, with a far lower characteristic frequency than 1 Hz. Therefore dielectric spectroscopy was carried out in the frequency range of 200 μ Hz to 50 mHz by investigating the complex permittivity of the material. The complex permittivity is defined by the expression:

$$\hat{\epsilon} = \epsilon' + j\epsilon'' \quad (1)$$

where ϵ' and ϵ'' are defined as the real and imaginary parts of permittivity since the former depicts the strength of the dipoles in the material aligning themselves when an external electric field is applied. This part is known as permittivity characterizing the electric energy stored within the dielectric material [36,37]. The imaginary permittivity represents the losses in the material due to conduction and polarization. The dissipation factor or $\tan \delta$ is the ratio of the imaginary and real parts of permittivity ($\tan \delta = \epsilon''/\epsilon'$). Modeling a relaxation process by the Debye model, the real and imaginary parts of permittivity as a function of angular frequency can be expressed by the following equations:

$$\epsilon'(\omega) = \epsilon_{\infty} + \frac{\epsilon_s - \epsilon_{\infty}}{1 + (\frac{\omega}{\omega_0})^2} \quad (2)$$

$$\epsilon''(\omega) = \frac{(\epsilon_s - \epsilon_{\infty})(\frac{\omega}{\omega_0})}{1 + (\frac{\omega}{\omega_0})^2} \quad (3)$$

where the ϵ_s and ϵ_{∞} are the permittivities at 0 and infinity frequency, at the same time, ω_0 is the characteristic angular frequency of the relaxation process. The relationship between ϵ_s and ϵ_{∞} can be seen in Figure 3. As the figure shows, the imaginary part of permittivity has a peak at the characteristic frequency, i.e., loss peak. Where the imaginary part has the peak, the changing of the real part is the highest. By changing the characteristic frequency, the curves shift together. The complex permittivity also enables the determination of the conductivity of the material. However, ϵ'' contains the sum of resistive and dielectric losses, if the resistive part is dominant, the slope of $\epsilon(\omega)$ is ω^{-1} and $\epsilon''(\omega)$ is constant in the dielectric spectrum [38]. At very low frequencies (below 1 Hz), the dc conduction is the dominant part of dielectric loss in XLPE cable insulation [39].

The measurements were carried out with Omicron Dirana (Omicron Electronics GmbH, Klaus, Austria). This equipment uses the combination of frequency-domain spectroscopy (FDS) and polarization-depolarization current (PDC) methods to determine the dielectric response. The equipment directly measures the dielectric response in the frequency domain at higher frequencies by the FDS technique. To determine the response in the lower frequency range, time-domain PDC data are recorded. Then, the PDC data are converted to the frequency domain by using discrete Fourier transformation. This technique has an important advantage, namely, it reduces the measurement time by 73% [38,40]. The accuracy of the equipment is 2% below 1 mHz for power and dissipation factor measurement and 0.5% for capacitance.

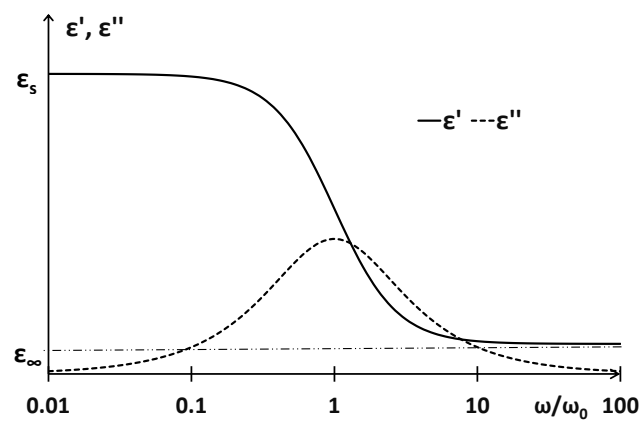
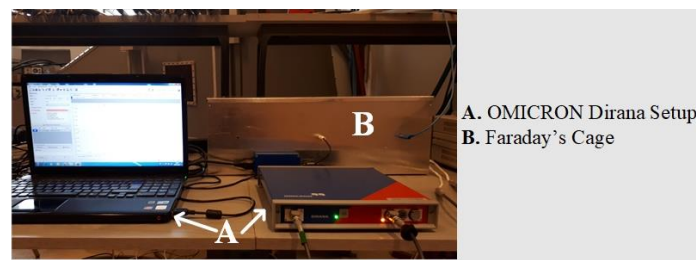
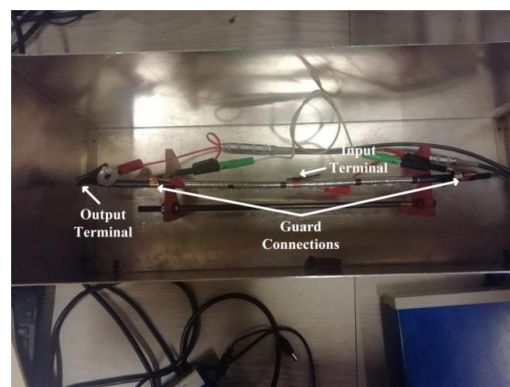


Figure 3. The relationship between real (ϵ') and imaginary (ϵ'') parts of permittivity in case of one Debye relaxation.

Since the subject of the investigation is a single core unshielded cable, the measurement of dielectric properties requires an external electrode, which was prepared by wrapping alumina foil around the cable. The voltage source, the equipment terminal, was connected to the external foil electrode through a copper strip. In contrast, the current output was connected to the internal conductor, as the measurement setup is shown in Figure 4. This connection ensures the lowest noise in the result. The cable samples were placed in the Faraday's cage connected to the guard for more noise suppression.



(a)



(b)

Figure 4. The test setup: (a) Omicron Dirana equipment; (b) cable sample in the Faraday's cage.

2.4. Shore D Hardness Measurement

The hardness measurement is based on the indentation depth of the indenter foot into the material applying a constant force. If the indentation is the highest, the measured value is 100, and if there is no indentation, the result is 0. In the case of the Shore D scale, the force is 4450.0 mN, the maximum penetration distance is 2.54 mm, and a 30-degree conical pressure foot is used. The Shore D hardness measurement is suitable for testing flat samples with a minimum 6 mm thickness according to the ASTM D2240-05 standard [41].

Therefore in this research, the Shore D hardness was tested as a comparative measurement to investigate the mechanical properties.

The hardness of the cable was measured at the ends and center with a total of 10 measuring points at 25 ± 0.5 °C. Although the test method is suitable for the flat samples [41], with the adaption of the foot adapter, the measurement can be executed for the round surfaces. In this investigation, the Shore D hardness measures the resultant hardness of the jacket and the insulation.

3. Results

3.1. Dielectric Spectroscopy

3.1.1. Thermal Aging

The measurement result of the real part of permittivity (ϵ') for the thermal stress is plotted against the frequency for each period in Figure 5a. According to the general behavior of dielectrics, the ϵ' decrease as the frequency increase. This characteristic behavior of the ϵ' was the same for all the aging periods. With aging time, the ϵ' either decreased or remained constant at all frequencies, except at 2×10^{-2} Hz and above, where a slight increase was observed. This behavior can be explained by the comparison with the imaginary parts curves.

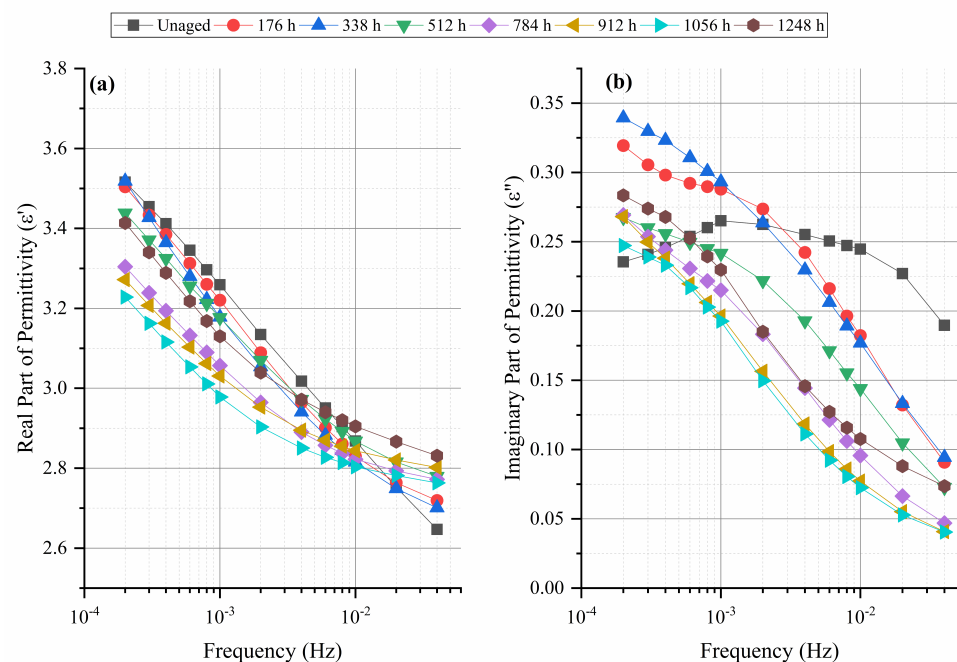


Figure 5. (a) Real and (b) imaginary parts of permittivities for thermal aging.

The results of the imaginary part of permittivity (ϵ'') are plotted in Figure 5b. The rearrangement of curves in the frequency range suggests that the ϵ'' curves shift towards a lower frequency range with aging, indicating the conductivity decrease with aging. This behavior explains the decreasing of ϵ'' values at the lowest frequencies. In the case of the unaged sample, the ϵ'' started with a certain value, then increased with the increase in frequency and reached a maximum value, and then again started to decrease. With thermal aging, the ϵ'' increased between 2×10^{-4} Hz and 1×10^{-3} Hz for the first two thermal aging periods, and then ϵ'' decreased with aging time. For frequency higher than 1×10^{-3} Hz there was a decreasing trend in the values of ϵ'' . This behavior was observed until the sixth thermal aging period (1056 h), whereas the values increased at all frequency points.

3.1.2. Thermo-Mechanical Aging

The ϵ' in the case of the T-M aging is shown in Figure 6a. The behavior of the ϵ' against frequency was similar to the thermal stress, irrespective of the aging. In contrast, the observed impact of T-M was as the ϵ' increased after the first two periods for the whole frequency spectrum, while it started to decrease after the third period (507 h). A slight increase after the sixth period (1051 h) was observed, while a substantial decrease in the whole curve was noted after the seventh T-M period.

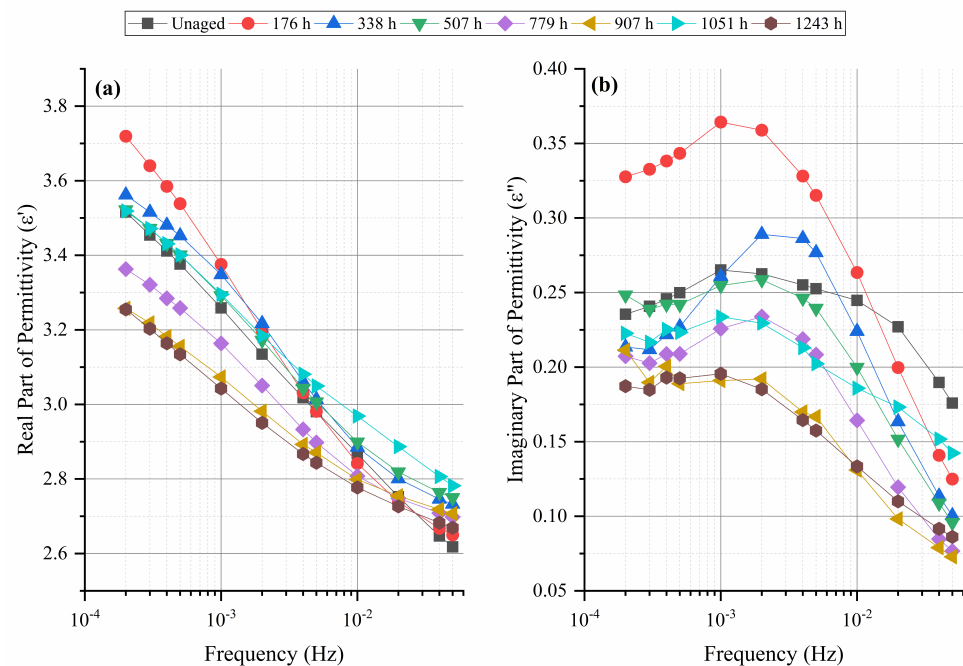


Figure 6. (a) Real and (b) imaginary parts of permittivities for thermo-mechanical aging.

The frequency plot of ϵ'' values is shown in Figure 6b. For almost all aging periods, ϵ'' started with a particular value. Then, the imaginary part of permittivity increased with frequency, reached a peak value at a specific frequency, and then declined with a further frequency increase. A noticeable increase in the values was noted in the ϵ'' after the first T-M period between 2×10^{-4} Hz and 1×10^{-3} Hz, while at higher frequencies, the values decreased. After a longer aging time, the ϵ'' decreased at all frequencies till the fifth T-M period (907 h). Like the ϵ' , after 1051 h, the ϵ'' increased, which then decreased after the last aging round.

3.2. Shore D Hardness

The Shore D hardness recorded results of the cable under thermal and thermo-mechanical aging have been plotted in Figure 7. An overall increase in the hardness of the cable was also observed for thermal and thermo-mechanical aging. However, the hardness increase is higher in thermo-mechanical aging, which suggests the combined stress has a more intensive effect on the material structure, which results in higher hardness values.

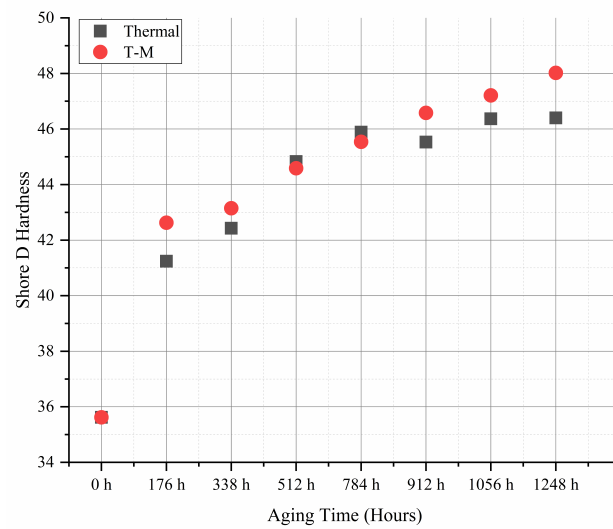


Figure 7. Shore D hardness against aging time thermal and thermo-mechanical (T-M) aging.

4. Discussion

The increase in ϵ' in a very-low-frequency range (below 1 Hz) is associated with the electrode polarization when the charge carriers accumulate near the electrodes, increasing the apparent value of the dielectric constant [42]. While the ϵ'' is a component related to the dielectric loss [43,44], one can expect that with aging, an increase in the losses will be experienced with the degradation of the polymer. Three frequencies were selected to simplify the analysis of the results: 200 μ Hz, 1 mHz, and 10 mHz, and the behavior of both kinds of aging were studied. The plot of the ϵ' and ϵ'' for each stress at the selected frequencies is shown in Figure 8.

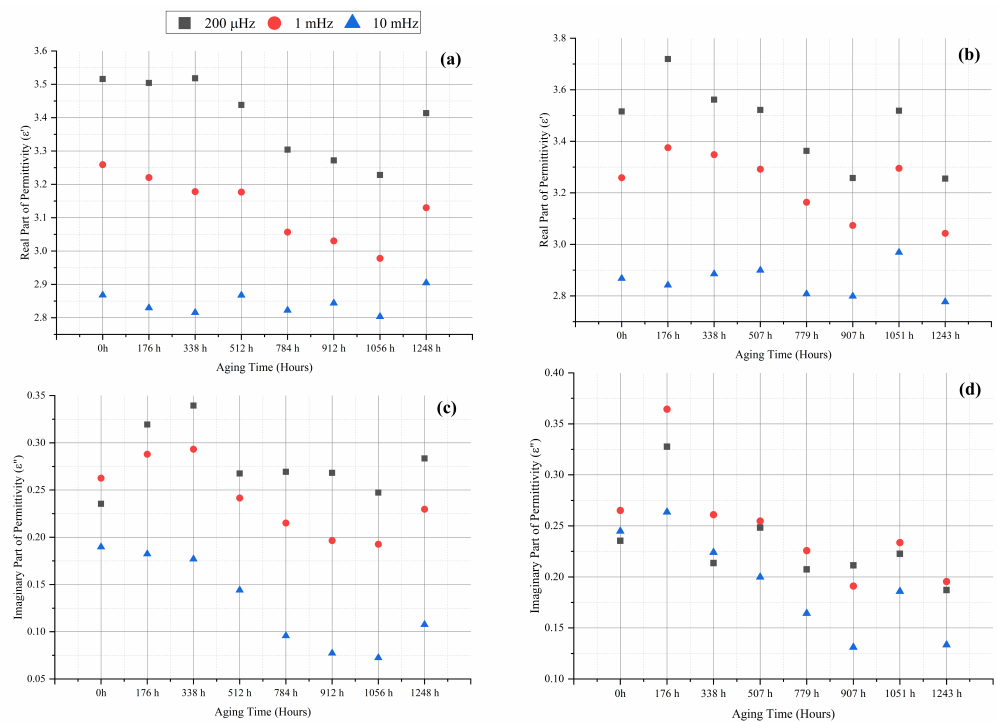


Figure 8. Real part of permittivity for (a) thermal aging, and (b) thermo-mechanical aging; imaginary part of permittivity for (c) thermal aging, and (d) thermo-mechanical aging at selected frequencies.

Under thermal aging, the ϵ' at the selected frequencies decreased with aging. After the last aging period, it increased, at 10 mHz, the ϵ' value even exceeded the unaged value.

Under T-M aging, at 200 μHz and 1 mHz, an initial increase in the ϵ' was observed, then the ϵ' started to decrease with more aging times. In contrast, different behavior is seen at 10 mHz, where the real part of permittivity dropped after the first period. Then ϵ' increased until the third period. More aging periods resulted in a decrease in the ϵ' values. A surprising behavior was observed under the T-M aging after the sixth period, where the values of the ϵ' increased even higher than the unaged values, which then decreased after the seventh period.

The effect of thermal stress on the ϵ'' caused an increase in the values for the first two periods at only 200 μHz and 1 mHz, which then declined with more aging, but at 10 mHz the values linearly decreased. The last thermal aging period resulted in a substantial increase in the values. At 200 μHz the value of ϵ'' remained higher than the unaged ones for all the aging periods.

While the T-M stress resulted in the increase in the ϵ'' after the first stress period at 1 mHz and 10 mHz, then it decreased with aging. In comparison, a clear trend was not observed at 200 μHz , where only the first and third periods affected the increase in the values higher than the unaged ones. Like the ϵ' , the ϵ'' values increased at all the selected frequencies after the sixth thermal period, whereas after the seventh thermal period, the values decreased.

The loss peak frequencies are also plotted for thermal and thermo-mechanical aging (Figure 9). For an unaged cable sample, a polarization peak was observed at 1 mHz, which with aging, was shifted to 200 μHz Figure 9a. Nevertheless, the curves of Figure 5b suggest in the case of aged samples, the peak of the polarization peak should be below 200 μHz . In the case of the T-M stress, the polarization peak did not change its position after the first aging period. However, it shifted to a higher frequency of 2 mHz until the fourth aging period and then to 200 μHz after the fifth aging period, Figure 9b. At the same time, it shifted back to 1 mHz after the sixth period and remained as it for the seventh period.

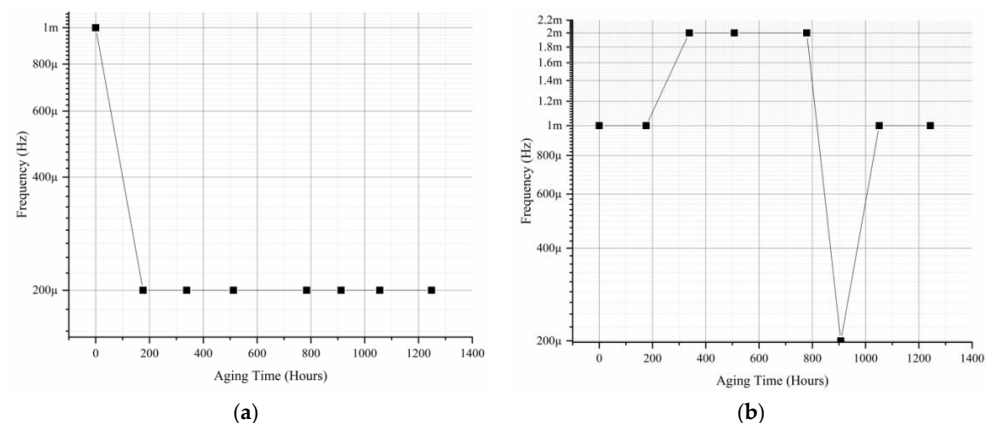


Figure 9. Shifting of the maximum value of the imaginary part of permittivity under (a) thermal, and (b) thermo-mechanical aging.

For a more detailed analysis of the dependence of real and imaginary parts of permittivity curves on aging, and similarly to [30,45], four deducted quantities have been calculated, namely the central real and imaginary parts of permittivity (*CRP* and *CIP*), and the real and imaginary permittivities' central frequencies (*RPCF* and *IPCF*). The *CRP* is calculated by summing up the multiplication of the logarithm of the frequencies by the measured ϵ' values at given frequencies and dividing this sum by the sum of the logarithm of the frequencies, as it can be seen in Equation (4).

$$CRP = \frac{\sum_{i=1}^n \log_{10} f_i \epsilon'_i(f_i)}{\sum_{i=1}^n \log_{10} f_i} \quad (4)$$

By changing the ϵ' to ϵ'' in Equation (4), the *CIP* can be calculated:

$$CIP = \frac{\sum_{i=1}^n \log_{10} f_i \epsilon_i''(f_i)}{\sum_{i=1}^n \log_{10} f_i} \quad (5)$$

The *RPCF* can be calculated as the average of the permittivity values weighted by the logarithm of the frequency:

$$RPCF = 10^{\frac{\sum_{i=1}^n \log_{10} f_i \epsilon_i'(f_i)}{\sum_{i=1}^n \log_{10} f_i}} \quad (6)$$

By changing the ϵ' to ϵ'' in the Equation (6), the *IPCF* can be calculated:

$$IPCF = 10^{\frac{\sum_{i=1}^n \log_{10} f_i \epsilon_i''(f_i)}{\sum_{i=1}^n \log_{10} f_i}} \quad (7)$$

These deduced quantities make spectroscopy curves evaluate easier since two numbers characterize the shifting of the curves. *CRP* and *CIP* are the characteristic values for real and imaginary permittivity changes over the frequency range of investigation. *RPCF* and *IPCF* characterise the shift of the curves in the frequency range. The change of *CRP* *RPCF* with aging is Figure 10.

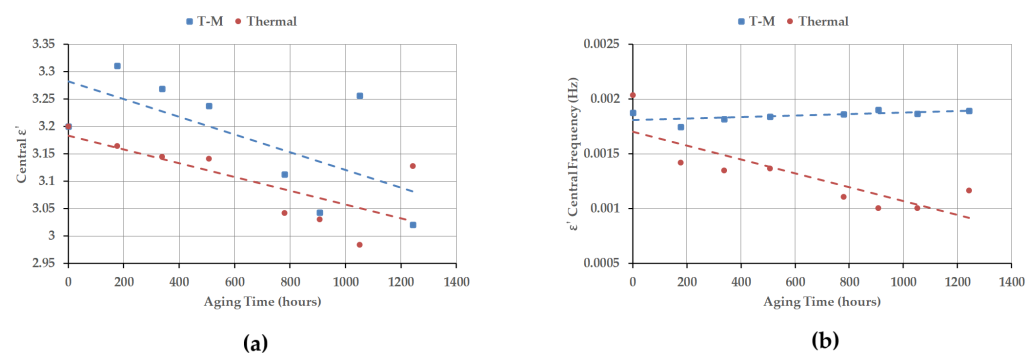


Figure 10. The calculated deduced quantities to characterize the $\epsilon'(f)$ curves (a) central real part of permittivity (*CRP*); (b) real part of permittivity's central frequency (*RPCF*).

Figure 10a shows that *CRP* of thermally aged samples decreases with aging from the initial 3.2 below 3. However, after the last aging round, it jumps up to almost 3.15. In the case of thermo-mechanically aged samples, the *CRP* has increased over 3.3 after the first aging round. Then, it decreases. The fitted trendlines show that the real part of the permittivity for the T-M samples was higher by nearly 0.1 during the whole aging period in the investigated frequency range.

The *CRP* curve of thermally aged samples shows a monotonous decreasing trend with aging, while the *CRP* of thermo-mechanically aged samples does not change (Figure 10b). Accordingly, the curves of the real part of permittivity of thermally aged samples shift towards lower frequencies, while there is no significant change in the case of T-M samples.

In general, the *CIP* and *IPCF* values clearly show the changing of an average loss in the investigated frequency range and the changing of the average polarization peak with aging. The values of *CIP* and *IPCF* are depicted in Figure 11.

Figure 11a shows the *CIP* change with aging in case thermal and T-M aging. In both cases, the dielectric loss increases at the beginning of aging. The *CIP* increases in the first two aging periods of thermal aging. A more significant increase can be observed in the first aging period of T-M aging, then the *CIP* values decrease. By calculating the linear trend, no significant difference can be observed between thermal and T-M *CIP* values. The *IPCF* values (Figure 11b) were dropped by 0.5 mHz after the first aging round, then the *IPCF* of thermally aged samples decreased, while that of T-M samples shows a small variation, a minimal decreasing trend can be observed. The calculated linear trends suggest

the $IPCF$ values of T-M samples are higher 0.5 mHz at the ending of aging. The trendlines show the ϵ'' curves shifted towards higher frequencies in the case of T-M aging. Hence the polarisation peaks are at higher frequencies than the thermally aged samples.

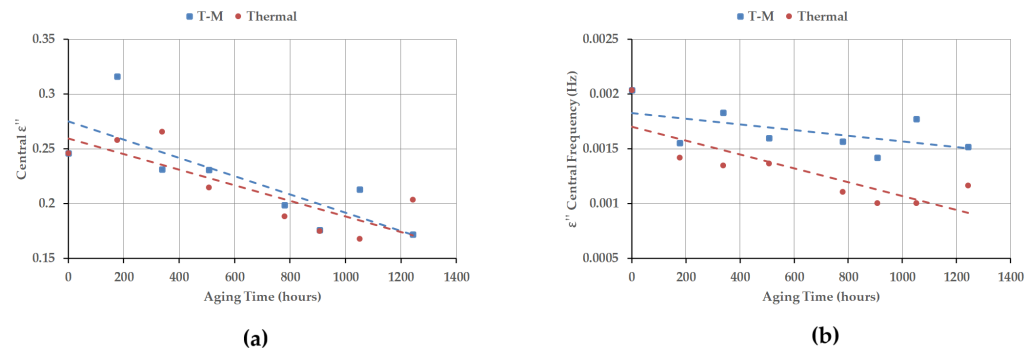


Figure 11. The calculated deduced quantities to characterize the $\epsilon''(f)$ curves (a) central imaginary part of permittivity (CIP); (b) imaginary part of permittivity's central frequency (IPCF).

The comparison of the change in Shore D hardness of thermally and thermo-mechanically aged samples has been drawn in Figure 7. For most of the aging periods (176 h, 338 h, 912 h, 1056 h, and 1248 h), the increases in hardness were 19.7%, 21.2%, 30.8%, 32.61%, and 34.89%, respectively, for T-M in comparison to 15.78%, 19.12%, 27.82%, 30.18% and 30.26% for thermal only. Hence, the thermo-mechanical stress has resulted in more hardness of the cable than the thermal stress only.

Under the thermal stress in the presence of oxygen, it is believed that the polymer undergoes molecular structural changes due to the cross-linking, chain scission, and oxidation reactions, which occur at the same time in the crystalline and amorphous regions. The actual cause of the degradation of the polymer depends on the dominance of one of these reactions. The cross-linking reaction generates a solid network that opposes the external field's effect and restrains the dipoles' movements, which is a case opposite to the chain scission reaction.

However, a very simple cable was chosen for the experiment, from the point of view of aging, the subject of the experiment is a complex structure. It contains two layers made from different polymers; moreover, the inner XLPE is covered by the CSPE jacket. Therefore, during the accelerated aging, the XLPE insulation was not contacted directly with the air. By investigating cable jacket samples removed from commercial cables, the significant effect of diffusion-limited oxidation (DLO) on the degradation of CSPE cable jacket material has been reported at temperatures as low as 110 °C [46]. Consequently, in the case of intact cable samples, when the air contacts only the outer surface of samples, it can be assumed the CSPE jacket consumes oxygen during aging at elevated temperatures. Therefore, the oxidative degradation of the XLPE insulation was very limited; hence, cross-linking and recrystallization were the main degradation mechanisms [47].

In addition to these reactions, materials such as CSPE, which has chlorine and sulfur dioxide attached to the polyethylene backbone, undergo dehydrohalogenation. During dehydrohalogenation, the halogen atom is separated from the polymer chain and the hydrogen, resulting in double bonds in the polymer chain [48,49], resulting in increased conductivity and permittivity [50].

Under the exclusive mechanical stress, it has been reported that the polymer may experiences two stresses: tension and compression [14]. The former assists the movement of the molecular chain, which may lead to the fracture of the chain and could increase the microcavities size [51,52]. It has also been reported that this would also increase the space charges. In contrast, the compression stress acts opposite to the tension, where the molecular chains come close to each other and support the bond attraction leading to more stabilization. This also inhibits the increase in the intensity of space charges. Since in our case, the cable has been exposed to both thermal and mechanical stresses, where the

inner side of the cable is under compression force and the outer side under tension force, Figure 12. Therefore, cross-linking and chain scission reactions in the presence of oxygen under thermal stress are also playing their role.

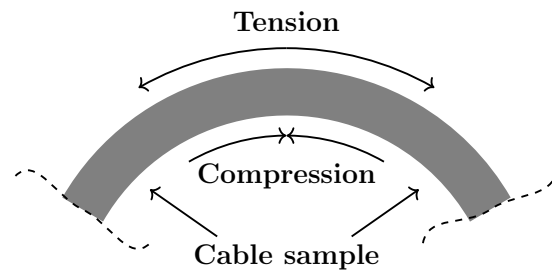


Figure 12. Tension and compression stresses on a bended cable sample.

The cable insulation's hardness increase under both types of stresses is also related to the reason that at elevated temperature, the generated small molecules due to decomposition reactions re-cross link with each other and increase the cable's hardness [47]. This phenomenon in the presence of compression stress due to mechanical aging is reinforced.

From the point of dielectric measurement view, the insulation and the jacket of non-shielded, single-core cables are considered a layered arrangement. Hence, the applied electrode arrangement (covering the cable's surface by conductive foil) can investigate only the resultant dielectric properties, i.e., the real and imaginary parts of permittivities, of the layers. Similarly, the Shore D hardness also measures the resultant hardness of both layers. Since the degradation processes also increase the hardness of the CSPE and the XLPE, the result will also be an increasing trend in thermal and T-M aging cases. However, conductivity and permittivity of CSPE increase due to thermal aging, the resultant dielectric loss and permittivity decrease in the investigated frequency range according to the change of CIP values. Nevertheless, degradation processes of the XLPE, namely the cross-linking and recrystallization, decrease its conductivity and permittivity [53]. Since the thickness of the XLPE insulation is higher by 50%, the resultant values of the real and imaginary parts of permittivities are significantly affected by the XLPE. The annealing effect of XLPE can cause the initial increase in CIP. The annealing effect increases the conductivity of XLPE at the beginning of thermal treatment [54].

It can be concluded that the parallel thermal-mechanical stress results in more intensive degradation of the mechanical properties of cable insulation than the thermal stress alone. Since the layered structure of jacket and insulation makes it difficult to identify the degradation processes and analyze the dielectric behavior. Further studies, including chemical analysis, are needed to reveal the degradation mechanism of single-core LV cables. This study would be beneficial to point out the importance of applying combined mechanical-thermal stressing for accelerated aging testing in the qualification procedure of NPP cables.

5. Conclusions

The main purpose of the work was to compare the dielectric behavior in-low-frequency range and Shore D hardness of thermally and thermo-mechanically aged single-core CSPE/XLPE insulated LV NPP cables. For the purpose of investigation, one group of samples was straightened, and the other one was coiled on a cylinder. Both groups of samples were aged at 120 °C for more than 1200 h. The dielectric spectrum in the 200 μHz to 50 mHz range and the Shore D hardness were measured on both groups. By analyzing the dielectric spectra, the real and imaginary parts of permittivities changed differently in both groups although, they did not show a clear trend with aging. To clarify the changes in the dielectric spectrum due to aging, derived quantities, namely, the central real and imaginary parts of permittivity and the real and imaginary permittivities' central frequency were introduced. The deducted quantities show that the real part of the permittivity of the

thermo-mechanically aged samples was higher by nearly 0.1 than that of thermally aged ones during the whole aging period in the investigated frequency range. The deducted quantities show that the real part of the permittivity of the thermo-mechanically aged samples was higher by nearly 0.1 than that of thermally aged ones during the whole aging period in the investigated frequency range. At the same time, the central frequency of the real part of permittivity curves decreased by 1 mHz due to thermal aging. A similar change was not observed on thermo-mechanically aged samples.

However, the central imaginary part of permittivity did not differ significantly between the groups, the imaginary permittivity's central frequency was higher by 0.5 mHz in the case of thermo-mechanically aged samples. This suggests a higher conductivity of thermo-mechanically aged samples, which can be the result of the annealing effect. During aging, the Shore D hardness was also higher on the thermo-mechanically aged samples than the thermally aged ones. At the end of aging, the hardness of the thermo-mechanically aged samples was 34% higher than the initial value, while that of the thermally aged samples was only 30% higher.

Based on the results, it can be concluded that mechanical stress has a strong impact on the degradation of the polymeric materials of the cable in combination with the thermal stress, which is considered during the simulation of service aging of cables. These results could lead to the inclusion of mechanical stress in the aging procedure of cable qualification, enabling the design of more robust cables in a harsh environment. For the future perspective, it is intended to carry out the chemical and other electrical and mechanical tests to further elaborate and understand the impact of mechanical stress with thermal stress on the LV cable aging.

Author Contributions: Conceptualization, R.S.A.A., E.M. and Z.Á.T.; investigation R.S.A.A., E.M. and Z.Á.T.; formal analysis, E.M.; writing—original draft preparation, E.M. and Z.Á.T.; visualization, E.M.; writing—review and editing, R.S.A.A. and Z.Á.T.; supervision, Z.Á.T.; funding acquisition, Z.Á.T. All authors have read and agreed to the published version of the manuscript.

Funding: Project no. 123672 has been implemented with the support provided by the National Research, Development and Innovation Fund of Hungary, financed under the KNN_16 funding scheme.

Data Availability Statement: The data presented in this study are available on request from the corresponding author.

Conflicts of Interest: The authors declare no conflict of interest.

References

1. International Atomic Energy Agency. *Energy, Electricity and Nuclear Power Estimates for the Period up to 2050*; Number 1 in Reference Data Series; International Atomic Energy Agency: Vienna, Austria, 2021.
2. International Atomic Energy Agency. *Assessing and Managing Cable Ageing in Nuclear Power Plants*; Number NP-T-3.6 in Nuclear Energy Series; International Atomic Energy Agency: Vienna, Austria, 2012.
3. International Atomic Energy Agency. *Safety of Nuclear Power Plants: Commissioning and Operation*; Number SSR-2/2 (Rev. 1) in Specific Safety Requirements; International Atomic Energy Agency: Vienna, Austria, 2016.
4. *IEEE Standard for Qualifying Electric Cables and Splices for Nuclear Facilities*; IEEE Std 383-2015 (Revision of IEEE Std 383-2003); IEEE: New York, NY, USA, 2015; pp. 1–27. [[CrossRef](#)]
5. Subudhi, M. *Literature Review of Environmental Qualification of Safety-Related Electric Cables: Summary of Past Work*; Technical Report NUREG/CR-6384-Vol1; Brookhaven National Lab.: Upton, NY, USA, 1996; Volume 1.
6. Gazdzinski, R.; Denny, W.; Toman, G.; Butwin, R. *Aging Management Guideline for Commercial Nuclear Power Plants, Electrical Cable and Terminations*; Sandia Labs Report, SAND96-0344; Sandia National Laboratories: Albuquerque, NM, USA, 1996.
7. Bustard, L.; Holzman, P. *Low-Voltage Environmentally-Qualified Cable License Renewal Industry Report: Revision 1*; Final Report; Electric Power Research Inst.: Palo Alto, CA, USA, 1994.
8. Chailan, J.F.; Boiteux, G.; Chauchard, J.; Pinel, B.; Seytre, G. Effects of thermal degradation on the viscoelastic and dielectric properties of chlorosulfonated polyethylene (CSPE) compounds. *Polym. Degrad. Stab.* **1995**, *48*, 61–65. [[CrossRef](#)]
9. Nanda, M.; Tripathy, D. Physico-mechanical and electrical properties of conductive carbon black reinforced chlorosulfonated polyethylene vulcanizates. *Express Polym. Lett.* **2008**, *2*, 855–865. [[CrossRef](#)]
10. Mustafa, E.; Afia, R.S.A.; Tamas, Z.Á. Condition Monitoring Uncertainties and Thermal–Radiation Multistress Accelerated Aging Tests for Nuclear Power Plant Cables: A Review. *Period. Polytech. Electr. Eng. Comput. Sci.* **2020**, *64*, 20–32. [[CrossRef](#)]

11. Suraci, S.V.; Fabiani, D.; Mazzocchetti, L.; Giorgini, L. Degradation Assessment of Polyethylene-Based Material Through Electrical and Chemical-Physical Analyses. *Energies* **2020**, *13*, 650. [[CrossRef](#)]
12. Mustafa, E.; Afia, R.S.A.; Tamus, Z.Á. Application of Non-Destructive Condition Monitoring Techniques on Irradiated Low Voltage Unshielded Nuclear Power Cables. *IEEE Access* **2020**, *8*, 166024–166033. [[CrossRef](#)]
13. Plaček, V.; Kohout, T.; Kábrt, J.; Jiran, J. The influence of mechanical stress on cable service life-time. *Polym. Test.* **2011**, *30*, 709–715. [[CrossRef](#)]
14. Afia, R.S.A.; Mustafa, E.; Tamus, Z.Á. Mechanical Stresses on Polymer Insulating Materials. In Proceedings of the 2018 International Conference on Diagnostics in Electrical Engineering (Diagnostika), Pilsen, Czech Republic, 4–7 September 2018; pp. 1–4. [[CrossRef](#)]
15. Ball, E.; Holdup, H.; Skipper, D.; Vecillio, B. *Development of Crosslinked Polyethylene Insulation for UV Cables*; CIGRE Paper; CIGRE: Paris, France, 1984; Volume 21.
16. Chen, W.; Allen, J.K.; Tsui, K.L.; Mistree, F. A Procedure for Robust Design: Minimizing Variations Caused by Noise Factors and Control Factors. *J. Mech. Des.* **1996**, *118*, 478–485. [[CrossRef](#)]
17. Petkovski, D.B. *Multivariable Control Systems Design: A Case Study of Robust Control of Nuclear Power Plants*; Pergamon Press: Oxford, UK, 1987.
18. Banavar, R.; Deshpande, U. Robust controller design for a nuclear power plant using H/sub /spl infin// optimization. *IEEE Trans. Nucl. Sci.* **1998**, *45*, 129–140. [[CrossRef](#)]
19. Vajpayee, V.; Becerra, V.; Bausch, N.; Deng, J.; Shimjith, S.; Arul, A.J. Robust-optimal integrated control design technique for a pressurized water-type nuclear power plant. *Prog. Nucl. Energy* **2021**, *131*, 103575. [[CrossRef](#)]
20. Pánek, D.; Orosz, T.; Karban, P. Artap: Robust Design Optimization Framework for Engineering Applications. In Proceedings of the 2019 Third International Conference on Intelligent Computing in Data Sciences (ICDS), Marrakech, Morocco, 28–30 October 2019; pp. 1–6. [[CrossRef](#)]
21. Orosz, T.; Rassölkin, A.; Kallaste, A.; Arsénio, P.; Pánek, D.; Kaska, J.; Karban, P. Robust Design Optimization and Emerging Technologies for Electrical Machines: Challenges and Open Problems. *Appl. Sci.* **2020**, *10*, 6653. [[CrossRef](#)]
22. Gadó, K.; Orosz, T. Robust and Multi-Objective Pareto Design of a Solenoid. *Electronics* **2021**, *10*, 2139. [[CrossRef](#)]
23. Karban, P.; Pánek, D.; Orosz, T.; Petrášová, I.; Doležel, I. FEM based robust design optimization with Agros and Ārtap. *Comput. Math. Appl.* **2021**, *81*, 618–633. [[CrossRef](#)]
24. Arvia, E.M.; Sheldon, R.T.; Bowler, N. A capacitive test method for cable insulation degradation assessment. In Proceedings of the 2014 IEEE Conference on Electrical Insulation and Dielectric Phenomena (CEIDP), Des Moines, IA, USA, 19–22 October 2014; pp. 514–517. [[CrossRef](#)]
25. Linde, E.; Verardi, L.; Fabiani, D.; Gedde, U. Dielectric spectroscopy as a condition monitoring technique for cable insulation based on crosslinked polyethylene. *Polym. Test.* **2015**, *44*, 135–142. [[CrossRef](#)]
26. Imperatore, M.V.; Fifield, L.S.; Fabiani, D.; Bowler, N. Dielectric spectroscopy on thermally aged, intact, poly-vinyl chloride/ethylene propylene rubber (PVC/EPR) multipolar cables. In Proceedings of the 2017 IEEE Conference on Electrical Insulation and Dielectric Phenomenon (CEIDP), Fort Worth, TX, USA, 22–25 October 2017; pp. 173–176. [[CrossRef](#)]
27. Sriraman, A.; Bowler, N.; Glass, S.; Fifield, L.S. Dielectric and Mechanical Behavior of Thermally Aged EPR/CPE Cable Materials. In Proceedings of the 2018 IEEE Conference on Electrical Insulation and Dielectric Phenomena (CEIDP), Cancun, Mexico, 21–24 October 2018; pp. 598–601. [[CrossRef](#)]
28. Suraci, S.V.; Fabiani, D.; Xu, A.; Roland, S.; Colin, X. Ageing Assessment of XLPE LV Cables for Nuclear Applications Through Physico-Chemical and Electrical Measurements. *IEEE Access* **2020**, *8*, 27086–27096. [[CrossRef](#)]
29. Suraci, S.V.; Fabiani, D.; Colin, X.; Roland, S. Chemical and electrical characterization of XLPE cables exposed to radio-thermal aging. In Proceedings of the 2020 IEEE 3rd International Conference on Dielectrics (ICD), Valencia, Spain, 5–31 July 2020; pp. 57–60. [[CrossRef](#)]
30. Afia, R.S.A.; Mustafa, E.; Tamus, Z.Á. Aging Mechanisms and Non-Destructive Aging Indicators of XLPE/CSPE Unshielded LV Nuclear Power Cables Subjected to Simultaneous Radiation-Mechanical Aging. *Polymers* **2021**, *13*, 3033. [[CrossRef](#)]
31. Mustafa, E.; Afia, R.S.A.; Nouini, O.; Tamus, Z.Á. Implementation of Non-Destructive Electrical Condition Monitoring Techniques on Low-Voltage Nuclear Cables: I. Irradiation Aging of EPR/CSPE Cables. *Energies* **2021**, *14*, 5139. [[CrossRef](#)]
32. Matsunami, U.; Mikami, M. Study on the ageing degradation diagnosis of electric cables based on indenter modulus method. *INSS J.* **2008**, *15*, 236–242.
33. McCarter, D.; Shumaker, B.; McConkey, B.; Hashemian, H. Nuclear power plant instrumentation and control cable prognostics using indenter modulus measurements. *Int. J. Progn. Health Manag.* **2015**, *6*. [[CrossRef](#)]
34. Hashemian, H.; Mcconkey, B.; Harmon, G.; Sexton, C. Methods for testing nuclear power plant cables. *IEEE Instrum. Meas. Mag.* **2013**, *16*, 31–36. [[CrossRef](#)]
35. International Atomic Energy Agency. *Benchmark Analysis for Condition Monitoring Test Techniques of Aged Low Voltage Cables in Nuclear Power Plants*; Number 1825 in TECDOC Series; International Atomic Energy Agency: Vienna, Austria, 2017.
36. Altındal Yerişkin, S.; Balbaşı, M.; Tataroğlu, A. Frequency and voltage dependence of dielectric properties, complex electric modulus, and electrical conductivity in Au/7% graphene doped-PVA/n-Si (MPS) structures. *J. Appl. Polym. Sci.* **2016**, *133*, 43827. [[CrossRef](#)]

37. Yıldız, D.E.; Dökme, İ. Frequency and gate voltage effects on the dielectric properties and electrical conductivity of Al/SiO₂/p-Si metal-insulator-semiconductor Schottky diodes. *J. Appl. Phys.* **2011**, *110*, 014507. [[CrossRef](#)]
38. Fofana, I.; Hadjadj, Y. Electrical-Based Diagnostic Techniques for Assessing Insulation Condition in Aged Transformers. *Energies* **2016**, *9*, 679. [[CrossRef](#)]
39. Fothergill, J.C.; Dodd, S.J.; Dissado, L.A.; Liu, T.; Nilsson, U.H. The measurement of very low conductivity and dielectric loss in XLPE cables: A possible method to detect degradation due to thermal aging. *IEEE Trans. Dielectr. Electr. Insul.* **2011**, *18*, 1544–1553. [[CrossRef](#)]
40. Koch, M.; Raetzke, S.; Krueger, M. Moisture diagnostics of power transformers by a fast and reliable dielectric response method. In Proceedings of the 2010 IEEE International Symposium on Electrical Insulation, San Diego, CA, USA, 6–9 June 2010; pp. 1–5. [[CrossRef](#)]
41. American Society for Testing and Materials. *ASTM D2240-05 Standard Test Method for Rubber Property: Durometer Hardness*; ASTM: West Conshohocken, PA, USA, 2010.
42. Min, D.; Yan, C.; Huang, Y.; Li, S.; Ohki, Y. Dielectric and Carrier Transport Properties of Silicone Rubber Degraded by Gamma Irradiation. *Polymers* **2017**, *9*, 533. [[CrossRef](#)]
43. Menczel, J.D.; Prime, R.B. *Thermal Analysis of Polymers: Fundamentals and Applications*; John Wiley & Sons: Hoboken, NJ, USA, 2009.
44. Jonscher, A.K. Dielectric relaxation in solids. *J. Phys. D Appl. Phys.* **1999**, *32*, R57–R70. [[CrossRef](#)]
45. Csányi, G.M.; Bal, S.; Tamas, Z.Á. Dielectric Measurement Based Deducted Quantities to Track Repetitive, Short-Term Thermal Aging of Polyvinyl Chloride (PVC) Cable Insulation. *Polymers* **2020**, *12*, 2809. [[CrossRef](#)] [[PubMed](#)]
46. Gillen, K.T.; Assink, R.; Bernstein, R.; Celina, M. Condition monitoring methods applied to degradation of chlorosulfonated polyethylene cable jacketing materials. *Polym. Degrad. Stab.* **2006**, *91*, 1273–1288. [[CrossRef](#)]
47. Zhang, Y.; Wu, Z.; Qian, C.; Tan, X.; Yang, J.; Zhong, L. Research on Lifespan Prediction of Cross-Linked Polyethylene Material for XLPE Cables. *Appl. Sci.* **2020**, *10*, 5381. [[CrossRef](#)]
48. Mustafa, E.; Ádám, T.Z.; Afia, R.S.A.; Asipuella, A. Thermal Degradation and Condition Monitoring of Low Voltage Power Cables in Nuclear Power Industry. In *Technological Innovation for Industry and Service Systems*; Camarinha-Matos, L.M., Almeida, R., Oliveira, J., Eds.; Springer International Publishing: Cham, Switzerland, 2019; pp. 405–413.
49. York, R.J.; Ulrich, J.B.; Murphy, G.; Prather, D.G. *Mitigation of Aging in Low Voltage Power Cables in Nuclear Power Plants*; University of Tennessee: Knoxville, TN, USA, 2015.
50. Lee, J.H.; Kang, M.K.; Jeon, J.S.; Lee, S.H.; Kim, I.Y.; Park, H.S.; Shin, Y.D. A study on the properties of CSPE according to accelerated thermal aging years. *J. Electr. Eng. Technol.* **2014**, *9*, 643–648. [[CrossRef](#)]
51. Du, B.X.; Xu, H.; Li, J. Effects of mechanical stretching on space charge behaviors of PP/POE blend for HVDC cables. *IEEE Trans. Dielectr. Electr. Insul.* **2017**, *24*, 1438–1445. [[CrossRef](#)]
52. Du, B.X.; Su, J.G.; Han, T. Effects of mechanical stretching on electrical treeing characteristics in EPDM. *IEEE Trans. Dielectr. Electr. Insul.* **2018**, *25*, 84–93. [[CrossRef](#)]
53. Chi, X.; Li, J.; Ji, M.; Liu, W.; Li, S. Thermal-Oxidative Aging Effects on the Dielectric Properties of Nuclear Cable Insulation. *Materials* **2020**, *13*, 2215. [[CrossRef](#)]
54. Diego, J.A.; Belana, J.; Orrit, J.; Cañadas, J.C.; Mudarra, M.; Frutos, F.; Acedo, M. Annealing effect on the conductivity of XLPE insulation in power cable. *IEEE Trans. Dielectr. Electr. Insul.* **2011**, *18*, 1554–1561. [[CrossRef](#)]